NANO LETTERS

pubs.acs.org/NanoLett Letter

Vibration-Driven Triboelectric Nanogenerator for Vibration Attenuation and Condition Monitoring for Transmission Lines

Shuangting Hu, Zhihao Yuan, Ruonan Li, Zhi Cao, Hanlin Zhou, Zhiyi Wu,* and Zhong Lin Wang*

Cite This: https://doi.org/10.1021/acs.nanolett.2c01912 Read Online

ACCESS | Metrics & More | Article Recommendations | Supporting Information

ABSTRACT: Vibration is an omnipresent energy source that is renewable and has the potential to cause damage to transmission lines. Harvesting harmful vibration energy can achieve vibration attenuation. Here, a vibration-driven triboelectric nanogenerator (V-TENG) with the potential for vibration attenuation is proposed as a power source for monitoring the operating condition of transmission lines. The V-TENG with structural optimization and frequency response range improvement is first discussed, indicating that it has a simple structural design with a good output performance. Then an energy management circuit is used to improve the charging efficiency of large capacitors. The vibration attenuation effect and wireless transmission system are verified in the simulation environment, benefiting from the well-designed structure and outstanding electric performance. This work demonstrates an efficient strategy for harvesting vibration energy through the TENG, which provides valuable guidance for further construction of online monitoring of transmission lines.

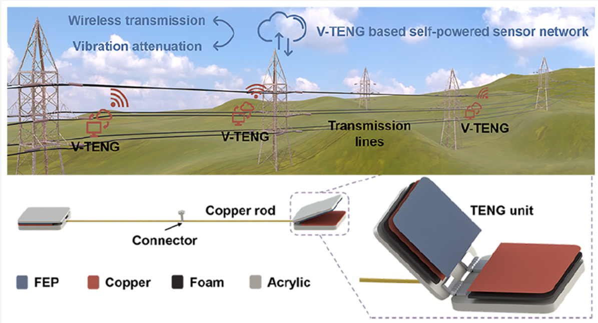

KEYWORDS: *triboelectric nanogenerator, vibration energy harvesting, vibration attenuation, transmission line, energy management circuit, wireless transmission system*

With the threat of global warming and energy crises, searching for renewable energy resources is one of the most urgent challenges to the sustainable development of human civilization.[1−4] As a renewable distributed energy source, vibrational energy can be harvested and converted into electrical energy.[5−7] Over the past decade, it has been an appealing target for energy harvesting as a potential alternative to the battery. However, most vibration energy is wasted due to the difficulty of harvesting it. In some cases, it may even be highly destructive.[8,9] For instance, the transmission lines are vulnerable to aeolian vibration. Transmission lines play an essential role in energy transport and distribution as the arteries and veins of a power system.[10−12] If harnessed, this unused and harmful vibration energy can help realize the online monitoring of the running state of the transmission lines.[13]

Previous researchers have focused on using electromagnetic and piezoelectric generators to convert vibration energy into electricity.[14−17] They have shown exemplary performance in harvesting vibration energy. In 2012, the triboelectric nanogenerator (TENG), a new energy harvesting technology, was invented by Wang's group.[18−21] Thanks to the unique working mechanism, the TENG has been proven to be a simple, cost-effective, and efficient tool for efficient vibration energy harvesting, especially in the low-frequency region.[22−29] Multiple TENGs for vibration energy harvesting have been fabricated. The harvested energy has successfully driven small electronics such as light-emitting diode indicators, thermometers, and Bluetooth beacons.[30−33] The previous works are of great significance in promoting the wide application of the TENG, with most of them enhancing the response amplitude to increase the power generation. However, the enhanced vibration amplitude may be harmful in some engineering fields, such as transmission lines. As a result, vibration energy harvesting systems based on vibration enhancement are challenging to deploy in many settings that must reduce vibrations.[34−36]

This work proposes a vibration-driven triboelectric nanogenerator (V-TENG), preserving the largest power density among the previous works (Figure S1). Moreover, the V-TENG device can weaken the vibration energy. It is designed as a structure with TENG units fixed at both rods' ends. With the connector, the device can vibrate following the transmission line. This design is proven to reduce the vibration amplitude from 13 to 5 cm. In addition to mechanical properties, the output performance is systematically measured. The maximum open-circuit voltage, short-circuit current, and instantaneous power reach are 1002 V, 17.75 μA, and 4.31

Received: May 11, 2022
Revised: June 17, 2022

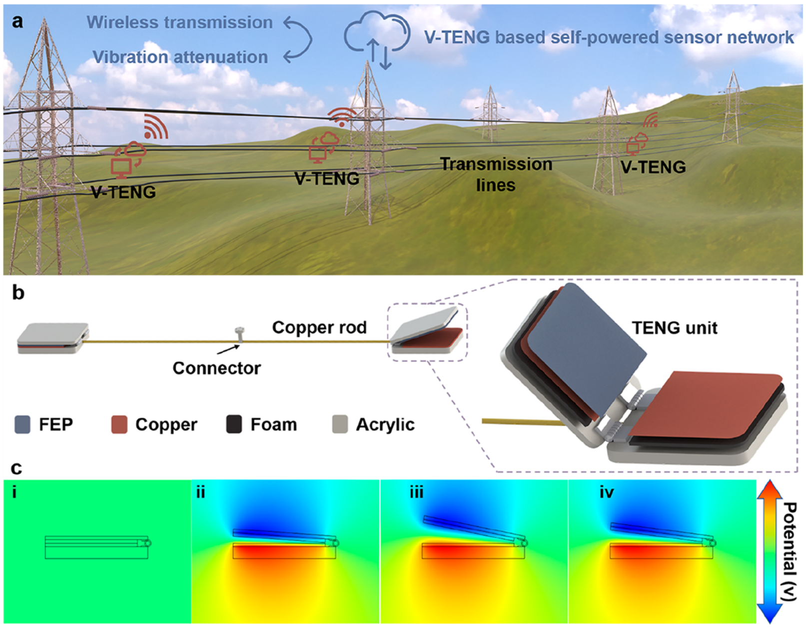

Figure 1. Structural design of the V-TENG. (a) Schematic diagram of the operating environment of the V-TENG. (b) Structure and material design of the V-TENG device. (c) Potential simulation results of four typical states in the working process.

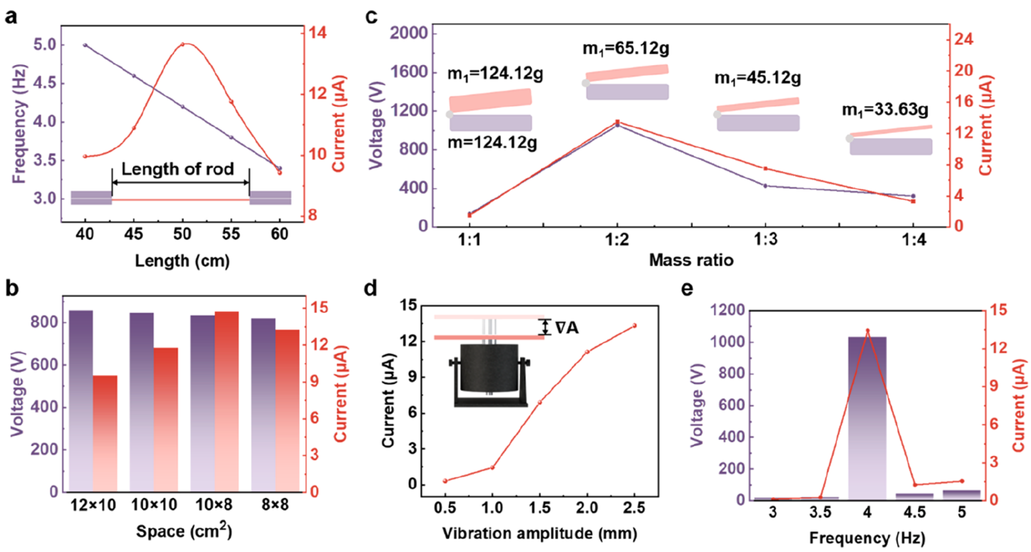

Figure 2. Electric characteristics and optimization of a single TENG. (a) Vibration frequency and output current are affected by the length of the rod. The output voltage/current influenced by the (b) space of tribolayers and (c) mass ratio of two substrates. (d) Change of output current with the increased vibration amplitude. (e) Change of output voltage/current under various vibration frequencies.

mW, respectively. The V-TENG maintains a stable output performance under a 4 Hz excitation, and the response frequency range can be broadened 5-fold by adding a movable mass roller. Furthermore, an energy management circuit based on an inductor is used to charge a 3.3 mF capacitor. With the powerful charging ability, advanced self-powered data transmission systems are developed. The emitted signal is operated through the management circuit, and the sensors can realize the automatic alarm function.

A gentle breeze may create aeolian vibrations on the transmission line. Although the amplitude of the transmission line is small under aeolian vibration, there will be fatigue damage if no antivibration measures are applied. As a result, the power line should take antivibration measures to prevent the vibration state. Figure 1a plots the schematic of a vibration energy harvester. The harvester can weaken the vibration amplitude of the transmission line and harvest low-frequency vibration energy. Figure 1b shows the component of the V-TENG. It comprises a copper rod, a connecting plate fixed to the transmission line, and two TENG units. The TENG unit is fabricated with acrylic plastic, foam, fluorinated ethylene propylene film (FEP, 50 μm), and copper film (30 μm). The copper film consists of a positive tribolayer and output electrode of the negative tribolayer. The negative friction layer of FEP is chosen because of its good electronic affinity. Moreover, the foam acts as a buffer layer, which is laminated between the copper electrode and acrylic substrate. Figure S1 schematically illustrates the working mechanism of the TENG. In the initial state, the copper electrode and FEP surface have positive and negative charges, respectively, due to the

https://doi.org/10.1021/acs.nanolett.2c01912
Nano Lett. XXXX, XXX, XXX−XXX

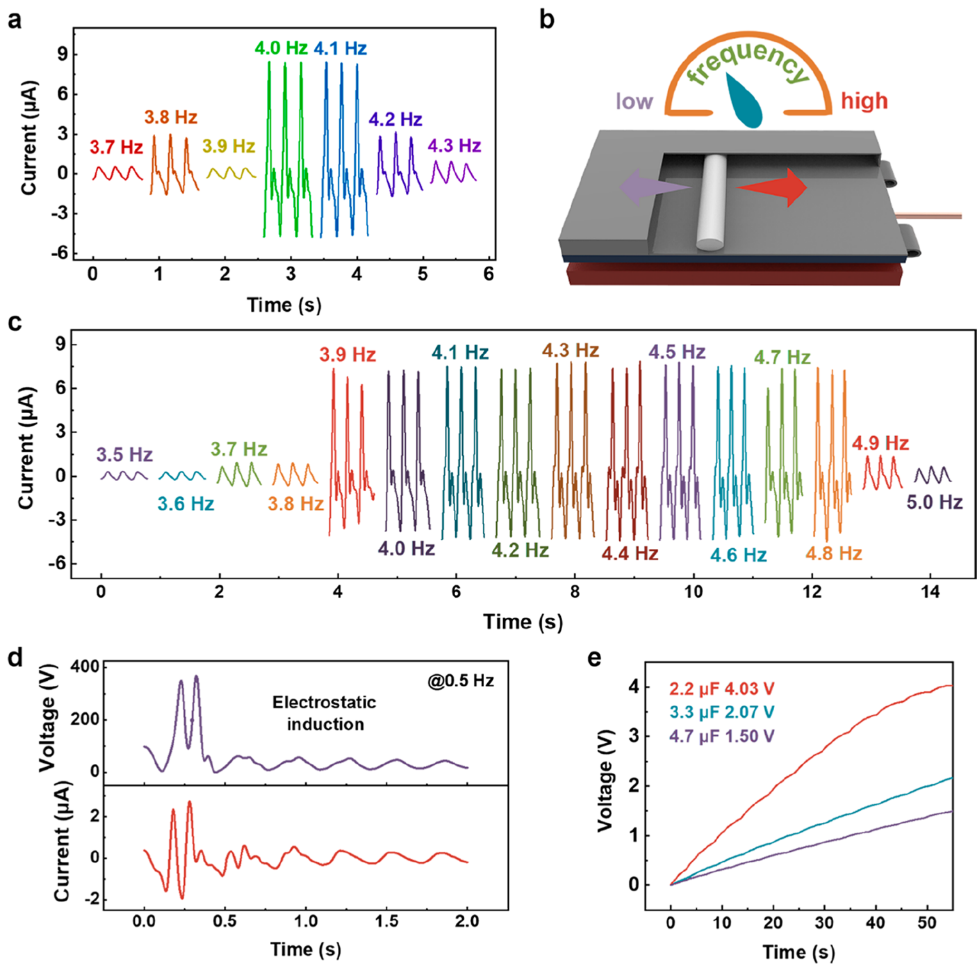

Figure 3. Resonant frequency optimization of the V-TENG. (a) Operating frequency range of the original V-TENG. (b) Schematic diagram of the impact of the movable roller on the frequency. (c) Operating frequency range after adding a movable roller on the V-TENG. (d) Output performance and (e) charging performance of a single TENG unit at 0.5 Hz.

triboelectric effect (i). When the two tribolayers are separated under the external forces, the positive charges of the upper copper electrode flow to the bottom copper electrode by the external circuit, generating a downward current (ii). Then the upper layer completely separates from the bottom layer, and the total positive charges transfer to the bottom copper electrode (iii). Finally, the upper layer falls under gravity, and the positive charges flow in the opposite direction (iv). Furthermore, the electric potential simulation results obtained using COMSOL (see Note S1 for details) are employed to elucidate the working principle of the TENG (Figure 1c).

As the main component of connecting two TENG units, the length of the copper rod has a significant impact on output. The output frequency decreases when the length of the rod changes from 40 to 60 cm, and the output current of a single TENG unit increases first and then decreases, reaching the maximum value with the length of 50 cm (Figure 2a). Figure S2a shows the particular output current waveform under different lengths and the transferred charge exhibiting the same characteristics (Figure S2b). The results indicate that the length of the rod has an optimal value, ensuring sufficient contact separation. Meanwhile, the output of the TENG under different sizes is systematically studied (Figure 2b). The output voltage decreases slightly as the size decreases, whereas the output current increases and decreases and is greatly enhanced with the size of 10 cm × 8 cm. The trend of current change is contrary to the trend of size change, roughly. Although the internal resistance of the TENG increases with the size of the tribolayer, the voltage is almost constant, leading to a drop in current. Figure S3a,b plots the waveform of voltage and current. The time taken for the characteristic waveform to appear in three peaks decreases as the size decreases, indicating the improvement of the output frequency. In addition, the output voltage of the TENG exceeds the measuring range of 6514 electrometers, so the oscilloscope is used to measure the voltage value, which leads to the difference in the waveform. After the size of the tribolayer is determined, each layer is divided into two pieces, which is equivalent to connecting two 8 cm × 5 cm TENGs. There is no change in the characteristic output waveform compared to the original state (Figure S4a), and the charge quantity is also consistent (Figure S4b). It could be that the connection of the external circuit is the same as that before the tribolayer is separated. We can conclude that the method of separating the tribolayers in parallel does not help improve the output in TENG design. The mass ratio of the two tribolayers also plays an important role in TENG output (Figure 2c). With the mass ratio of 1:2, the output voltage and current are both enhanced. The typical output waveforms of various mass ratios are illustrated in Figure S5.

Figure 2d compares the output current when enlarging the amplitude of the electromagnetic shaker, which shows an approximately proportional relationship, but the characteristic

https://doi.org/10.1021/acs.nanolett.2c01912
Nano Lett. XXXX, XXX, XXX−XXX

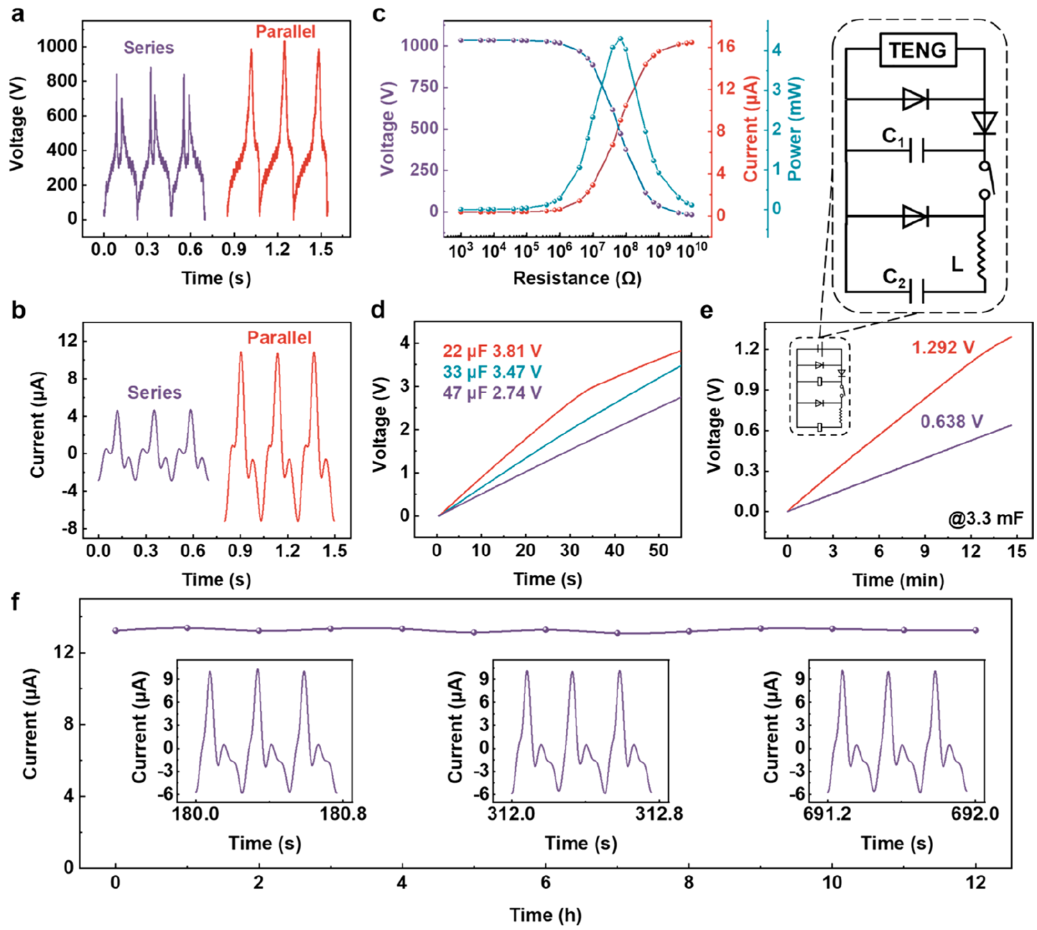

Figure 4. Output performance of the V-TENG. (a) Open-circuit voltage. (b) Short-circuit current of two TENG units connected parallel and series. (c) Load characteristics. (d) Charging performance of the TENG-P. (e) Charging performance of the V-TENG with an energy management circuit (in the box is the circuit diagram). (f) Results of the operation stability test during 12 h under excitation of 4 Hz.

of the waveform is different in Figure S6a. The upper tribolayer does not completely separate from the bottom, resulting in a small current fluctuation when the vibration amplitude is less than 1.5 mm. The degree of the upper tribolayer separating from the bottom increases as the amplitude increases, aggrandizing the output current. Moreover, the electromagnetic shaker delivers more momentum as the vibration amplitude increases and the current continues to rise. However, the transferred charge remains stable when the amplitude exceeds 2 mm (Figure S6b), suggesting the separation gap up to a maximum. Figure 2e exhibits the output voltage and current value under different vibration frequencies. The two show the same change trend, which first increases and then decreases as the frequency increases, acquiring an extreme at 4 Hz. At 4 Hz, the waveform is inconsistent with the others, indicating the TENG contacts and separates completely (Figure S7).

The TENG unit is tested at 0.1 Hz intervals. It achieves a maximum output at 4.0 and 4.1 Hz, meaning the working frequency range is only 0.2 Hz (Figure 3a). A narrow working frequency range affects the energy conversion efficiency of the TENG. Therefore, a movable roller is added on the upper tribolayer to adjust the barycenter position. The roller can roll along the direction of the copper rod so that the resonant frequency of the TENG can be autotunable (Figure 3b). When motived by the electromagnetic shaker, the TENG movable roller starts moving above the upper tribolayer. With the movement, the barycenter position changes, resulting in a change in the resonant frequency of the TENG. Once the TENG is excited at its resonant frequency, the roller acquires a unique position where there is minimal potential energy. The roller remains at this position until the excitation frequency changes, and it will adapt to a new position to acquire a minimum potential energy position again. For every change in excitation frequency, the movable roller position changes further. When the roller moves to the left with respect to the drawing, the resonant frequency decreases. On the contrary, the resonant frequency will enhance. The new working frequency range is plotted in Figure 3c. It has a great response in the 3.9−4.8 Hz range, 5 times wider than the original frequency range. In this way, the roller changes the barycenter position of the upper substrate to increase the working frequency band. Although the output is lower when the TENG works out of the resonant frequency, it still has good electric performance. Figure 3d shows that the output performance of the TENG is excited at 0.5 Hz. The upper tribolayer tends to separate from the bottom as soon as it is motivated, generating 386 V and 4.9 μA. Then it vibrates on the bottom tribolayer, and the output drops to 86 V and 1.2 μA due to the electrostatic induction. Figure 3e displays the charging performance of a single TENG unit working out of the resonant frequency (0.5 Hz). For capacitors with a capacitance of 2.2, 3.3, and 4.7 μF, the charging voltage can reach 4.03, 2.07, and 1.50 V, respectively, within 55 s.

https://doi.org/10.1021/acs.nanolett.2c01912
Nano Lett. XXXX, XXX, XXX−XXX

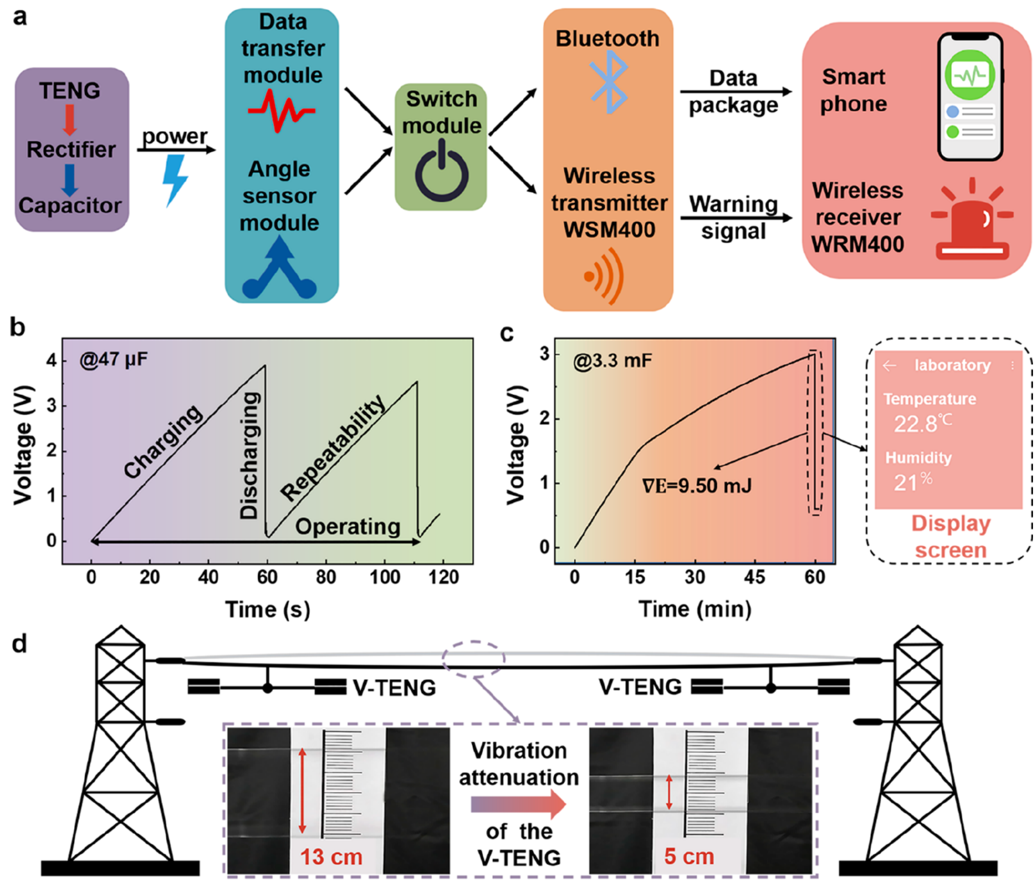

Figure 5. Application of the V-TENG. (a) Schematic illustration of the V-TENG-based wireless self-powered system. Typical working waveform of the (b) wireless self-powered alarm system and (c) wireless temperature and humidity monitoring. (d) Vibration attenuation of the V-TENG on the simulation transmission line.

The output of two TENG units can be connected in parallel or in series (denoted as TENG-P and TENG-S) to fully utilize the harvested vibration energy. Figure 4a depicts the output voltage of TENG-P and TENG-S at 4.3 Hz (median value of the new working frequency range). The series voltage (882 V) is lower than the parallel voltage (1002 V), and each waveform has two peaks, implying the two units have a phase difference. Similarly, the series current (7.48 μA) is much lower than the parallel current (17.75 μA) (Figure 4b). The equivalent resistance of the TENG in parallel increases more than twice that of the TENG in series. For the V-TENG, the parallel connection is a better choice. The electrical outputs of TENG-P when loading a resistor are characterized in the same test condition (Figure 4c). The instantaneous peak power is 4.31 mW at the matched resistance of 70 MΩ. The output voltage gradually increases and becomes saturated from low resistance to high resistance, while the output current represents an opposite trend. As a visual demonstration of performance, Figure S8 and Video S1 depict the application of powering 35 LEDs in a room from bright lighting conditions to dark conditions. Figure 4d further explores the charging behaviors of TENG-P. The voltages of 22, 33, and 47 μF capacitors are charged to 3.81, 3.47, and 2.74 V, respectively, within 55 s. However, the charging speed is slow for capacitors with large capacities (Figure S9). Since the output feature of the TENG is high pulsed voltage but low current capability, the capacitor will leak, which will gear down the charging speed. As a result, we introduce a power management circuit with an inductor (L), a voltage regulating capacitor (C_1), and a storage capacitor (C_2) to improve the charging efficiency. The electromagnetic shaker controls the switch, so the frequency of the switch is consistent with that of the shaker. Specifically, the shaker drives the V-TENG to the lowest point to separate the two tribolayers, and the V-TENG starts to generate electric energy and charges C_1. Then the shaker drives the V-TENG to the highest point and turns on the machinal switch, and the energy in both TENGs and C_1 transfers to L. Finally, the shaker drives the device downward and turns off the switch, resulting in the energy stored in L being transferred to C_2. A new cycle begins when the shake drives the V-TENG to the lowest point again. The 3.3 mF capacitor can be charged to 1.292 V in 15 min (Figure 4e). Compared to 0.638 V without the power management circuit, the charging speed has been improved significantly. In addition, output stability and mechanical durability are important features influencing output performance. The output current is recorded for 12 h under excitation of 4 Hz to evaluate the fatigue property of the V-TENG. With the protection of the buffer layer, the V-TENG maintains the original output performance for a long time. The negligible value variation in the process can be attributed to the influence of temperature and humidity on output performance. The insets of Figure 4f show the time-dependent current graphs at 3 h later (16 μA), about 6 h later (15.93 μA), and about 11 h later (15.99 μA), which further manifests the superb stability and durability of the V-TENG.

https://doi.org/10.1021/acs.nanolett.2c01912
Nano Lett. XXXX, XXX, XXX−XXX

Based on the powerful low-frequency vibration energy harvesting capability of the V-TENG, a self-powered system for data transfer and danger alarm can be developed. Figure 5a shows the external circuit and other function modules which comprise the system. The feasibility of the self-powered tilt alarm system and temperature/humidity data transferring system have been verified. An ultra-low-power consumption wireless transmitter, a switch, and an angle sensor make up the self-powered tilt alarm system. The vibration energy harvested by the V-TENG is saved in a capacitor (47 μF) through a rectifier bridge. When the inclination angle exceeds the trigger threshold, the switch module turns on immediately. Then the electric energy passes through the independent operating transmitter with a 433 MHz encoder (WSM400). Subsequently, the transmitter sends the warning signal through the antenna. After the receiver module (WRM400) receives the signal, it makes a bell ring. The typical operation waveform of the system is plotted in Figure 5b, which has a 3.3 V working voltage. It means that a charging voltage greater than 3.3 V ensures enough energy to power the circuit. The whole process is recorded in Video S2, and the repeatability of the system is also revealed. A low-energy Bluetooth module is the main component for the self-powered temperature and humidity data transferring system. As the V-TENG begins to operate, the capacitor is charged to 3 V in 1 h with the mentioned power management circuit (a 3.3 mF capacitor). Then the phone can obtain temperature and humidity data, and the voltage value drops to 0.7 V (Figure 5c). The voltage in the capacitor is too low to keep the thermometer on, but the Bluetooth module still transmits data to the phone wirelessly. It takes approximately 9.5 mJ of energy to complete the data transfer. The photo is shown in Figure S10, and the data transfer process is recorded in Video S3. In addition, other self-powered functions can be realized by replacing the module. Besides the application based on the electric output, the structure design of the V-TENG gives it the potential to dampen the vibration, which is verified. Figure 5d shows the vibration amplitude generated by the simulated transmission line under resonant frequency excitation (8 Hz), and the original vibration amplitude is about 13 cm. The equipment used in the vibration attenuation experiment of the simulated transmission line is shown in Figure S11. The V-TENG is fixed below the simulated transmission line. Despite the different resonant frequencies, the V-TENG does not achieve complete contact separation, but the vibration amplitude decreases suddenly to about 5 cm, which implies that the V-TENG device can weaken the vibration. The demonstration video is recorded as Video S4. The phenomenon means the V-TENG has the potential to effectively avoid fatigues, broken strands, and even broken wires in transmission lines.

A hybrid energy collector was designed and manufactured to collect vibration energy. The structure comprises a copper connecting rod and two TENG units. When the vibration occurs, the two layers of the substrate contact and separate to generate electricity. The V-TENG exhibited an output voltage of 1002 V, induced current of 17.75 μA, and output power of 4.31 mW at an amplitude of 2.5 mm. At the same time, a larger working band can be achieved by changing the length of the copper rod and adding a removable roller above it. The excellent output capacity is verified, and the circuit design significantly improves the charging speed to use the harvested energy better. The self-powered information detection/transmission/alarm system driven by the V-TENG is tested, and the technical feasibility of supplying power for the sensor is verified. Finally, the device can attenuate the vibration of the transmission line. Considering the extensibility of the V-TENG, transmission line self-supply systems can develop equipment networks of different sizes, which is of great value in transmission line research.

■ ASSOCIATED CONTENT

Supporting Information

The Supporting Information is available free of charge at https://pubs.acs.org/doi/10.1021/acs.nanolett.2c01912.

Video S1: Application of powering 35 LEDs (MP4)

Video S2: Demonstration of the self-powered alarm system (MP4)

Video S3: Demonstration of the self-powered data transferring system (MP4)

Video S4: Demonstration the vibration attenuation (MP4)

Parameter setting of the simulation calculation of V-TENG (Notes S1), experimental section, and Figures S1−S12 (PDF)

■ AUTHOR INFORMATION

Corresponding Authors

Zhong Lin Wang − *Beijing Institute of Nanoenergy and Nanosystems, Chinese Academy of Sciences, Beijing 101400, P.R. China; School of Nanoscience and Technology, University of Chinese Academy of Sciences, Beijing 100049, P.R. China; School of Materials Science and Engineering, Georgia Institute of Technology, Atlanta, Georgia 30332-0245, United States;* orcid.org/0000-0002-5530-0380; Email: zlwang@gatech.edu

Zhiyi Wu − *Beijing Institute of Nanoenergy and Nanosystems, Chinese Academy of Sciences, Beijing 101400, P.R. China; School of Mechanical and Electrical Engineering, Guilin University of Electronic Technology, Guilin 541004, P.R. China; School of Nanoscience and Technology, University of Chinese Academy of Sciences, Beijing 100049, P.R. China;* orcid.org/0000-0002-3215-0092; Email: wuzhiyi@binn.cas.cn

Authors

Shuangting Hu − *Beijing Institute of Nanoenergy and Nanosystems, Chinese Academy of Sciences, Beijing 101400, P.R. China; School of Mechanical and Electrical Engineering, Guilin University of Electronic Technology, Guilin 541004, P.R. China*

Zhihao Yuan − *Beijing Institute of Nanoenergy and Nanosystems, Chinese Academy of Sciences, Beijing 101400, P.R. China*

Ruonan Li − *Beijing Institute of Nanoenergy and Nanosystems, Chinese Academy of Sciences, Beijing 101400, P.R. China*

Zhi Cao − *Beijing Institute of Nanoenergy and Nanosystems, Chinese Academy of Sciences, Beijing 101400, P.R. China*

Hanlin Zhou − *Beijing Institute of Nanoenergy and Nanosystems, Chinese Academy of Sciences, Beijing 101400, P.R. China*

Complete contact information is available at: https://pubs.acs.org/10.1021/acs.nanolett.2c01912

https://doi.org/10.1021/acs.nanolett.2c01912
Nano Lett. XXXX, XXX, XXX−XXX

Author Contributions

Z.W. and Z.L.W. conceived the idea and supervised the experiment. S.H. and Z.Y. prepared the manuscript. S.H. and R.L. designed the structure of the device. Z.C. performed the data measurements. H.Z. offered assistance with the experiments. All of the authors discussed the results and commented on the manuscript and contributed to the manuscript preparation.

Notes

The authors declare no competing financial interest.

■ ACKNOWLEDGMENTS

The research was supported by the National Natural Science Foundation of China (61503051).

■ REFERENCES

(1) Xue, G. B.; Xu, Y.; Ding, T. P.; Li, J.; Yin, J.; Fei, W. W.; Cao, Y. Z.; Yu, J.; Yuan, L. Y.; Gong, L.; Chen, J.; Deng, S. Z.; Zhou, J.; Guo, W. L. Water-evaporation-induced electricity with nanostructured carbon materials. *Nat. Nanotechnol.* **2017**, *12* (4), 317−321.

(2) Dunn, B.; Kamath, H.; Tarascon, J. M. Electrical Energy Storage for the Grid: A Battery of Choices. *Science* **2011**, *334* (6058), 928−935.

(3) Liu, C.; Li, F.; Ma, L. P.; Cheng, H. M. Advanced Materials for Energy Storage. *Adv. Mater.* **2010**, *22* (8), E28.

(4) Dresselhaus, M. S.; Thomas, I. L. Alternative energy technologies. *Nature* **2001**, *414* (6861), 332−337.

(5) Gupta, R. K.; Shi, Q. F.; Dhakar, L.; Wang, T.; Heng, C. H.; Lee, C. Broadband Energy Harvester Using Non-linear Polymer Spring and Electromagnetic/Triboelectric Hybrid Mechanism. *Sci. Rep.* **2017**, *7*, 41396.

(6) Chen, J.; Wang, Z. L. Reviving Vibration Energy Harvesting and Self-Powered Sensing by a Triboelectric Nanogenerator. *Joule* **2017**, *1* (3), 480−521.

(7) Zou, H. X.; Zhang, W. M.; Li, W. B.; Wei, K. X.; Gao, Q. H.; Peng, Z. K.; Meng, G. Design and experimental investigation of a magnetically coupled vibration energy harvester using two inverted piezoelectric cantilever beams for rotational motion. *Energy Convers. Manage.* **2017**, *148*, 1391−1398.

(8) Proso, U.; Slavic, J.; Boltezar, M. Vibration-fatigue damage accumulation for structural dynamics with non-linearities. *Int. J. Mech. Sci.* **2016**, *106*, 72−77.

(9) Fan, Z. W.; Jiang, Y.; Zhang, S. F.; Chen, X. Experimental Research on Vibration Fatigue of CFRP and Its Influence Factors Based on Vibration Testing. *Shock. Vib.* **2017**, *2017*, 1241623.

(10) Yuan, Z. H.; Wei, X. L.; Jin, X.; Sun, Y. G.; Wu, Z. Y.; Wang, Z. L. Magnetic energy harvesting of transmission lines by the swinging triboelectric nanogenerator. *Mater. Today Energy* **2021**, *22*, 100848.

(11) Jin, X.; Yuan, Z. H.; Shi, Y. P.; Sun, Y. G.; Li, R. N.; Chen, J. H.; Wang, L. F.; Wu, Z. Y.; Wang, Z. L. Triboelectric Nanogenerator Based on a Rotational Magnetic Ball for Harvesting Transmission Line Magnetic Energy. *Adv. Funct. Mater.* **2022**, *32* (10), 2108827.

(12) Yan, Q. Z.; Zhou, C. M.; Feng, X. B.; Deng, C.; Hu, W. Y.; Xu, Y. M. Galloping Vibration Monitoring of Overhead Transmission Lines by Chirped FBG Array. *Photonic Sens.* **2022**, *12* (3), 220310.

(13) Wu, H.; Wang, J. Y.; Wu, Z. Y.; Kang, S. L.; Wei, X. L.; Wang, H. Q.; Luo, H.; Yang, L. J.; Liao, R. J.; Wang, Z. L. Multi-Parameter Optimized Triboelectric Nanogenerator Based Self-Powered Sensor Network for Broadband Aeolian Vibration Online-Monitoring of Transmission Lines. *Adv. Energy Mater.* **2022**, *12* (13), 2103654.

(14) Wang, X.; John, S.; Watkins, S.; Yu, X. H.; Xiao, H.; Liang, X. Y.; Wei, H. Q. Similarity and duality of electromagnetic and piezoelectric vibration energy harvesters. *Mech. Syst. Signal Process* **2015**, *52*−*53*, 672−684.

(15) Naifar, S.; Bradai, S.; Viehweger, C.; Kanoun, O. Survey of electromagnetic and magnetoelectric vibration energy harvesters for low frequency excitation. *Measurement* **2017**, *106*, 251−263.

(16) Lei, Y. M.; Wen, Z. Y. Study on effects of the damping ratio on output performance of micro electromagnetic vibration energy harvesters. *Microsyst. Technol.* **2015**, *21* (1), 221−226.

(17) Ma, T. B.; Ding, Y. J.; Wu, X. D.; Chen, N. N.; Yin, M. H. Research on piezoelectric vibration energy harvester with variable section circular beam. *J. Low Freq. Noise V. A* **2021**, *40* (2), 753−771.

(18) Wang, Z. L. Triboelectric Nanogenerators as New Energy Technology for Self-Powered Systems and as Active Mechanical and Chemical Sensors. *ACS Nano* **2013**, *7* (11), 9533−9557.

(19) Fan, F. R.; Tang, W.; Wang, Z. L. Flexible Nanogenerators for Energy Harvesting and Self-Powered Electronics. *Adv. Mater.* **2016**, *28* (22), 4283−4305.

(20) Fan, F. R.; Tian, Z. Q.; Wang, Z. L. Flexible triboelectric generator! *Nano Energy* **2012**, *1* (2), 328−334.

(21) Shan, C.; Liu, W.; Wang, Z.; Pu, X.; He, W.; Tang, Q.; Fu, S.; Li, G.; Long, L.; Guo, H.; Sun, J.; Liu, A.; Hu, C. An inverting TENG to realize the AC mode based on the coupling of triboelectrification and air-breakdown. *Energy Environ. Sci.* **2021**, *14* (10), 5395−5405.

(22) Han, M. D.; Zhang, X. S.; Liu, W.; Sun, X. M.; Peng, X. H.; Zhang, H. X. Low-frequency wide-band hybrid energy harvester based on piezoelectric and triboelectric mechanism. *Sci. China Technol. Sci.* **2013**, *56* (8), 1835−1841.

(23) Wang, X. F.; Niu, S. M.; Yin, Y. J.; Yi, F.; You, Z.; Wang, Z. L. Triboelectric Nanogenerator Based on Fully Enclosed Rolling Spherical Structure for Harvesting Low-Frequency Water Wave Energy. *Adv. Energy Mater.* **2015**, *5* (24), 1501467.

(24) Liu, H.; Fu, H.; Sun, L.; Lee, C.; Yeatman, E. M. Hybrid energy harvesting technology: From materials, structural design, system integration to applications. *Renew. Sust. Energy Rev.* **2021**, *137*, 110473.

(25) Hou, C.; Chen, T.; Li, Y.; Huang, M.; Shi, Q.; Liu, H.; Sun, L.; Lee, C. A rotational pendulum based electromagnetic/triboelectric hybrid-generator for ultra-low-frequency vibrations aiming at human motion and blue energy applications. *Nano Energy* **2019**, *63*, 103871.

(26) Shi, Q.; Sun, Z.; Zhang, Z.; Lee, C. Triboelectric Nanogenerators and Hybridized Systems for Enabling Next-Generation IoT Applications. *Research* **2021**, *2021*, 6849171.

(27) Guo, X.; He, T.; Zhang, Z.; Luo, A.; Wang, F.; Ng, E. J.; Zhu, Y.; Liu, H.; Lee, C. Artificial Intelligence-Enabled Caregiving Walking Stick Powered by Ultra-Low-Frequency Human Motion. *ACS Nano* **2021**, *15* (12), 19054−19069.

(28) Shi, Q.; Wu, H.; Wang, H.; Wu, H.; Lee, C. Self-Powered Gyroscope Ball Using a Triboelectric Mechanism. *Adv. Energy Mater.* **2017**, *7* (22), 1701300.

(29) Guo, X.; Liu, L.; Zhang, Z.; Gao, S.; He, T.; Shi, Q.; Lee, C. Technology evolution from micro-scale energy harvesters to nanogenerators. *J. Micromech. Microeng.* **2021**, *31* (9), 093002.

(30) Chuan, W.; He, H.; Shuo, Y.; Chenxing, F. Research on the self-powered downhole vibration sensor based on triboelectric nanogenerator. *Proc. Inst. Mech. Eng. C.J. Mech. Eng. Sci.* **2021**, *235* (22), 6427−6434.

(31) Chen, J.; Zhu, G.; Yang, W. Q.; Jing, Q. S.; Bai, P.; Yang, Y.; Hou, T. C.; Wang, Z. L. Harmonic-Resonator-Based Triboelectric Nanogenerator as a Sustainable Power Source and a Self-Powered Active Vibration Sensor. *Adv. Mater.* **2013**, *25* (42), 6094−6099.

(32) Li, S. X.; Liu, L.; Zhao, Z. H.; Zhou, L. L.; Yin, X.; Li, X. Y.; Gao, Y. K.; Zhang, C. G.; Zhang, Q.; Wang, J.; Wang, Z. L. A Fully Self-Powered Vibration Monitoring System Driven by Dual-Mode Triboelectric Nanogenerators. *ACS Nano* **2020**, *14* (2), 2475−2482.

(33) Shan, C.; He, W.; Wu, H.; Fu, S.; Tang, Q.; Wang, Z.; Du, Y.; Wang, J.; Guo, H.; Hu, C. A High-Performance Bidirectional Direct Current TENG by Triboelectrification of Two Dielectrics and Local Corona Discharge. *Adv. Energy Mater.* **2022**, 2200963.

(34) Du, Y.; Deng, J. L.; Li, P.; Wen, Y. M. Energy transfer and redistribution: An approach for unifying vibrational energy harvesting and vibration attenuation. *Nano Energy* **2020**, *78*, 105245.

(35) Shen, W. A.; Zhu, S. Y.; Zhu, H. P. Experimental study on using electromagnetic devices on bridge stay cables for simultaneous energy

harvesting and vibration damping. *Smart Mater. Struct.* **2016**, *25* (6), 065011.
(36) Khan, F. U.; Ali, T. A piezoelectric based energy harvester for simultaneous energy generation and vibration isolation. *Int. J. Energy Res.* **2019**, *43* (11), 5922−5931.

https://doi.org/10.1021/acs.nanolett.2c01912
Nano Lett. XXXX, XXX, XXX−XXX